ACS APPLIED MATERIALS & INTERFACES

Research Article

www.acsami.org

Expanding the Redox Range of Surface-Immobilized Metallocomplexes Using Molecular Interfaces

Brian L. Wadsworth, Diana Khusnutdinova, Jennifer M. Urbine, Ahlea S. Reyes, and Gary F. Moore*

School of Molecular Sciences and the Biodesign Institute Center for Applied Structural Discovery (CASD), Arizona State University, Tempe, Arizona 85287-1604, United States

Supporting Information

ABSTRACT: Rationally designed material interfaces offer opportunities to control matter and energy across multiple length scales, yet remain challenging to synthetically prepare. Inspired by nature, where specific amino acid residues and soft-material coordination environments regulate the midpoint potentials of metal centers in proteins during enzymatic reactions, thin-film polymeric coatings have been developed to assemble molecular components, including catalysts, onto solid-state (semi)conducting surfaces. In this report, we describe the immobilization of metalloporphyrins onto transparent conductive oxide supports using either direct grafting to the oxide surface or coordination to an initially applied thin-film polypyridyl coating. The composite materials enable direct measurements of electrochemical and optical properties associated with the surface-immobilized components. Despite the similarity of the core cobalt porphyrin units used in assembling these hybrid architectures, the redox potentials assigned to the $Co^{III/II}$ relays span a 350 mV range across the distinct constructs. This range in redox potential is extended to 960 mV when including comparisons to constructs utilizing polymer-immobilized cobaloxime catalysts in place of cobalt porphyrins, where reduction of the cobaloximes requires significantly more-negative bias potentials. This work illustrates the use of soft-material interfaces for assembling molecular-modified electrodes where the nanoscale connectivity of the surface coatings determines the electrochemical properties of the macroscopic assemblies.

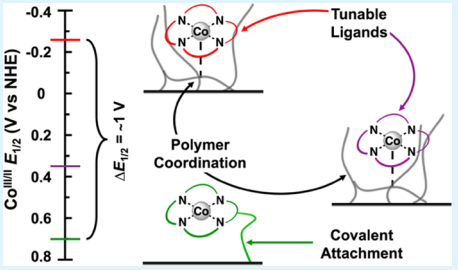

KEYWORDS: *molecular interfaces, surface immobilization, coordinating polymers, optoelectronics, porphyrins*

INTRODUCTION

Interfaces are central to the electronic properties, and hence performance, of materials in biology and technology.[1−6] In the technological realm, the emergence of new materials with applications to organic light-emitting diodes, organic solar cells, and thin-film coatings for catalysis has spurred interest in molecular interfaces composed of organic and/or inorganic components.[7−16] Although strategies for designing such interfaces promise the ability to chemically tailor the structural and physical properties of surfaces,[17−23] developing methods to effectively assemble soft-to-hard matter interfaces and characterize the resulting hybrid materials remain challenging.[24] Related to this, advances in synthetic chemistry have provided researchers exquisite control over structure and functionality at the nanoscale; however, a complete understanding of extending that knowledge to material constructs with dimensions at the meso- and macroscales is lacking.

In biological assemblies, molecular co-factors and catalytic active sites are organized into hierarchical structures made from proteins where amino acid residues form three-dimensional coordination environments that control the redox properties of metal centers at catalytically active sites and along electron-transport chains. For example, cytochromes, which are heme-containing proteins that function as electron-transfer agents in myriad metabolic pathways, contain iron centers with midpoint potentials spanning a nearly 800 mV range.[25−28] This relatively wide range of potentials using a common metal center exemplifies the critical role amino acid side chains and surrounding structure serve in redox reactions involving proteins.[29,30] Although significant fundamental insights have been gleaned from studies involving proteins immobilized on electrodes, such assemblies are limited for industrial applications due to their fragility and relatively large per geometric area footprints per number of metal-center active sites.[31] Nonetheless, the ability to incorporate design principles realized from such studies into technological constructs has inspired researchers and enabled improved control over human-engineered catalysts and electron-transfer assemblies.[32−35]

In this report, we describe thin-film coatings of cobalt porphyrins on transparent conductive oxide (TCO) electrode surfaces. The electrodes are composed of nanostructured indium tin oxide (nanoITO), and the surface coatings are prepared using either (1) direct photochemical grafting of a synthetically modified porphyrin, 5,10,15,20-tetra-*p*-tolyl-2-(4-vinylphenyl)porphyrin cobalt(II) (**1**),[36] forming **CoPInano-ITO** electrodes, or (2) application of a photochemically grafted poly(vinylpyridine) (PVP) layer that is used to

Received: August 26, 2019
Accepted: November 3, 2019
Published: November 4, 2019

DOI: 10.1021/acsami.9b15286
ACS Appl. Mater. Interfaces XXXX, XXX, XXX−XXX

Scheme 1. Depiction of the Strategies Used to Assemble the Molecular-Modified nanoITO Electrodes

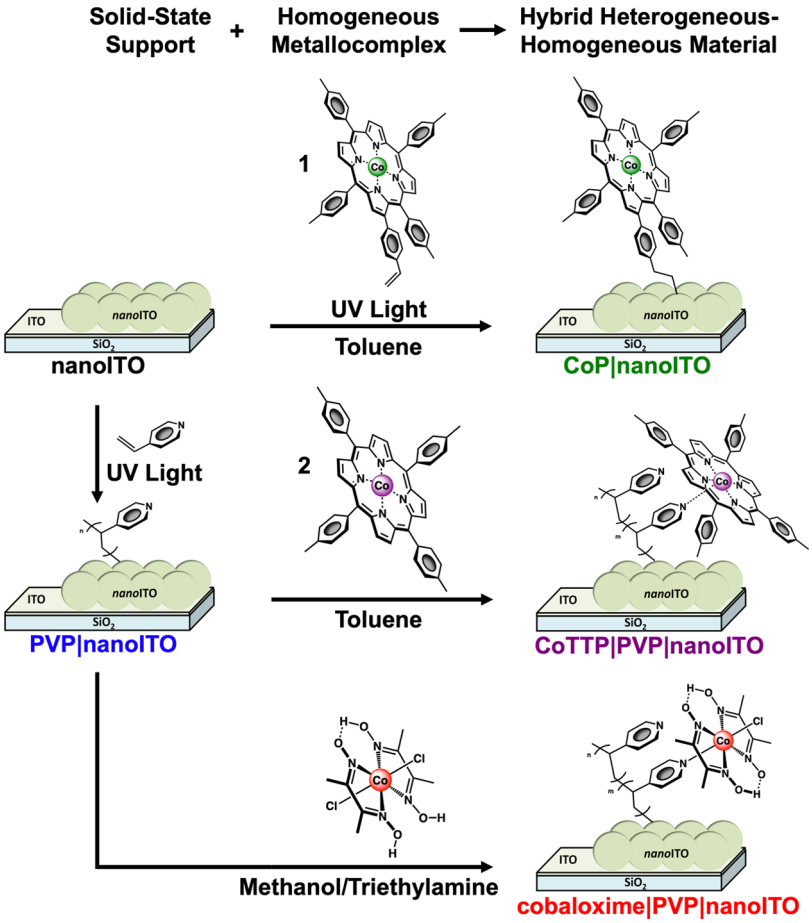

assemble 5,10,15,20-tetra-*p*-tolylporphyrin cobalt(II) (**2**) at nitrogen sites of the polymeric interface during a subsequent wet chemical processing step,[37,38] forming **CoTTP|PVP|nanoITO** electrodes. The transparent and conductive nature of the nanoITO supports enables comparisons of the electrochemical and optical properties of the heterogeneous–homogeneous porphyrin-containing constructs with those of homogeneous solutions of porphyrins as well as comparisons with a previously reported cobaloxime–poly(vinylpyridine)-nanostructured indium tin oxide (**cobaloxime|PVP|nanoITO**) assembly.[39] Thus, the nanoITO supports provide a tool for measuring and comparing redox properties associated with soft-material coatings that can be difficult or currently not possible to measure using semiconducting or insulating supports.

The findings presented herein show (1) cobalt porphyrins modified with a 4-vinylphenyl functional group at the β position of the macrocycles can be used as reagents (precursors) for achieving direct photochemical grafting of porphyrins onto the TCO surfaces, (2) initial application of a pyridyl-based polymer onto unmodified TCO surfaces enables immobilization of known molecular hydrogen-producing catalysts, including cobalt porphyrins and cobaloximes, via coordination to nitrogen sites along the surface-grafted polymer, (3) in both types of assemblies, the immobilized cobalt porphyrin units are redox active, (4) for **CoP|nanoITO** electrodes, the midpoint potentials of the redox features assigned to $Co^{III/II}$ and $Co^{II/I}$ couples of the surface-grafted cobalt porphyrin units are the same as those measured using homogeneous solutions of **2**, (5) for **CoTTP|PVP|nanoITO** electrodes, the potentials of the redox features assigned to $Co^{III/II}$ and $Co^{II/I}$ couples of the immobilized porphyrin units are cathodically shifted (350 and 150 mV for the $Co^{III/II}$ and $Co^{II/I}$ couples, respectively) as compared to those measured using **CoP|nanoITO** electrodes or homogeneous solutions of **2**, and (6) in comparison to previously reported **cobaloxime|PVP|nanoITO** electrodes, the **CoP|nanoITO** assemblies allow access to $Co^{III/II}$ and $Co^{II/I}$ redox chemistries at potentials 960 and 350 mV less negative, respectively.

RESULTS AND DISCUSSION

Material Preparation. Cobalt porphyrin-modified indium tin oxide (ITO) and nanoITO electrodes (**CoP|ITO** and **CoP|nanoITO**, respectively) were fabricated following a modified version of a method used to assemble cobalt porphyrins on gallium phosphide surfaces.[36] In this approach, a cobalt porphyrin modified with a 4-vinylphenyl functional group on the β position of the macrocycle is used as a reagent for preparing the porphyrin-modified samples via a one-step photochemical grafting method.

Cobalt porphyrin–poly(vinylpyridine)-modified ITO and nanoITO electrodes (**CoTTP|PVP|ITO** and **CoTTP|PVP|nanoITO**, respectively) were fabricated following a modified version of a two-step method used to assemble cobaloxime–poly(vinylpyridine)-modified ITO and nanoITO electrodes (**cobaloxime|PVP|ITO** and **cobaloxime|PVP|nanoITO**, respectively).[39] Briefly, freshly cleaned ITO or nanoITO electrodes (see Experimental Section for details) are placed

DOI: 10.1021/acsami.9b15286
ACS Appl. Mater. Interfaces XXXX, XXX, XXX–XXX

in an argon-sparged solution of 4-vinylpyridine and subjected to short-wavelength UV illumination (254 nm) for 2 h. The resulting polymer-functionalized electrodes are then ultrasonically cleaned in methanol for 2 min before exposing them to a solution of **2** in toluene under argon for 24 h (Scheme 1).

Following wet chemical processing, all resulting cobalt porphyrin-functionalized samples (**CoP|ITO**, **CoP|nanoITO**, **CoTTP|PVP|ITO**, and **CoTTP|PVP|nanoITO**) are rinsed with toluene, followed by rinsing with cleanroom isopropanol.

Characterization of Vibrational and Electronic Structure. Grazing angle attenuated total reflectance Fourier transform infrared (GATR–FTIR), X-ray photoelectron (XP), and ultraviolet–visible (UV–vis) spectroscopies were used to characterize materials described in this report. These measurements enable comparisons of the vibrational and electronic properties of the cobalt porphyrin components prior to surface immobilization and when immobilized via either direct grafting or coordination to pyridyl nitrogen sites along the initially applied PVP graft.

GATR–FTIR absorption spectra of **CoP|ITO** surfaces are characterized by a porphyrin planar deformation mode centered at 1001 cm^{-1} (Figure 1), a value identical to the

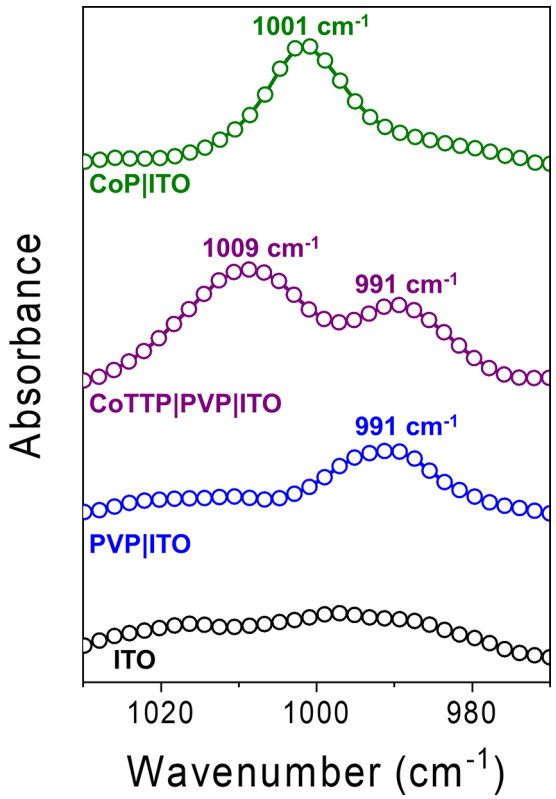

Figure 1. GATR–FTIR absorption spectra of **CoP|ITO** (green), **CoTTP|PVP|ITO** (purple), **PVP|ITO** (blue), and unfunctionalized ITO (black) from 1030 to 970 cm^{-1}.

vibrational frequency measured on surfaces of previously reported cobalt porphyrin-modified gallium phosphide electrodes that were prepared using the same porphyrin precursor (**1**).[36,40] In general, metalloporphyrins have distinct IR absorption bands in the 1014–1000 cm^{-1} range ascribed to in-plane deformations of the ring structure that are sensitive to both the elemental nature of the metal center and its local coordination environment.[37,40–42] For comparison, FTIR transmission spectra of **1** recorded in KBr also display an absorption band at 1001 cm^{-1} (assigned to the planar deformation mode) but feature an absorption band at 1626 cm^{-1} (assigned to a C=C vibration of the vinyl-functional group) that is not observed on surfaces of **CoP|ITO** (Figures S1 and S2). This lack of an absorption feature at 1626 cm^{-1} in spectra recorded using **CoP|ITO** samples is consistent with the proposed vinyl group grafting chemistry.[36] Further, unlike the polymeric immobilization strategy, surface attachment using the 4-vinylphenyl moiety does not require coordination or binding interactions involving the porphyrin metal center. Thus, the in-plane planar deformation mode is essentially unperturbed following immobilization, indicating the cobalt porphyrin maintains a 4-coordinate square planar geometry on the surface. The presence of intact porphyrin units on the surfaces of **CoP|ITO** samples is further confirmed by the presence of vibrational features associated with the C=C (1625–1525 cm^{-1}), C_α–N (1400–1300 cm^{-1}), and C_β–H (1200–1050 cm^{-1}) vibrations of the porphyrin macrocycle (Figure S2).

In contrast to the cobalt porphyrin planar deformation mode observed at 1001 cm^{-1} in spectra of **CoP|ITO**, spectra of **CoTTP|PVP|ITO** surfaces are characterized by a porphyrin planar deformation mode centered at 1009 cm^{-1} (Figure 1). This absorption feature is diagnostic of cobalt porphyrin complexes coordinated by an axial pyridyl group,[37,40] thus providing direct spectroscopic confirmation of successful attachment of the porphyrin components and information on the molecular nature of the connectivity. For comparison, the in-plane porphyrin deformation mode of **2** appears at 1003 cm^{-1} when measured in a matrix of KBr (Figure S1). In addition to the porphyrin deformation band at 1009 cm^{-1} on surfaces of **CoTTP|PVP|ITO**, an absorption feature centered at 991 cm^{-1} is also present and is ascribed to a ring-breathing mode of pyridyl groups on the surface.[37] We note that a similar absorption feature, also centered at 991 cm^{-1}, is present on the surfaces of **PVP|ITO** samples (Figure 1). The presence of intact polymer and porphyrin in samples of **CoTTP|PVP|ITO** is further confirmed by the presence of vibrational features associated with the C=N, C–N, and C–H vibrations of the surface-grafted PVP polymer (1600–1400 cm^{-1}) as well as C=C (1625–1525 cm^{-1}), C_α–N (1400–1300 cm^{-1}), and C_β–H (1200–1050 cm^{-1}) vibrations of the porphyrins (Figure S2).

XP spectra of **CoP|ITO** and **CoTTP|PVP|ITO** assemblies provide additional evidence of successful surface functionalization (Figures S3–S11). Survey spectra of both constructs show contributions from In, Sn, and O elements associated with the underpinning bulk ITO support as well as contributions from Co and N elements associated with immobilized cobalt porphyrins (Figures S4–S11). For **CoP|ITO** samples, analysis of the high-resolution Co $2p_{3/2}$ and N 1s spectral intensity ratios yields Co/N ratios of 1:4 (Figure S6), indicating no detectable loss of cobalt from the immobilized porphyrin units following UV-induced grafting. In the case of **CoTTP|PVP|ITO** samples, additional contributions from N elements associated with the surface-grafted polymer are present in the XP spectra, and the fraction of pyridyl sites on the polymer grafts that are coordinated to cobalt porphyrins can be estimated via evaluation of the Co 2p and N 1s high-resolution core-level spectra (vide infra).

Unlike N 1s core-level XP spectra collected using **PVP|ITO** samples, which are characterized by a single nitrogen feature

DOI: 10.1021/acsami.9b15286
ACS Appl. Mater. Interfaces XXXX, XXX, XXX–XXX

centered at 398.7 eV that is ascribed to contributions from pyridinic nitrogens of the surface-grafted polymer (Figure S8), N 1s core-level XP spectra collected using **CoTTP|PVP|ITO** samples can be fit with an additional component centered at 399.4 eV that is ascribed to contributions from pyrrolic nitrogens of the immobilized cobalt porphyrins as well as pyridinic nitrogens coordinated to cobalt centers of the immobilized porphyrins (Figures S10 and S11). Comparison of the relative intensities of Co 2p and N 1s core-level spectra as well as deconvolution of the N 1s core-level spectral contributions indicate that 25 ± 6% of the pyridyl units on the **CoTTP|PVP|ITO** surfaces are coordinated to a cobalt center. This estimate is limited by the inherent surface-sensitive nature of these measurements and assumes an even distribution of cobalt centers along the polymer grafts. Nonetheless, as described later in this report, the use of UV−vis spectroscopy, electrochemical techniques, and inductively coupled plasma mass spectrometry (ICP-MS) affords measurements of the per geometric area cobalt surface loadings and percentages of electroactive cobalt porphyrins that corroborate the X-ray photoelectron spectroscopy (XPS) results.

Information on the electronic structure of the immobilized porphyrin components was also obtained using UV−vis spectroscopy. Similar to absorption spectra of **2** dissolved in propylene carbonate, spectra of **CoP|nanoITO** electrodes immersed in propylene carbonate display single Soret and Q-band transitions positioned at 414 and 533 nm, respectively (Figures 2, S12−S14 and Table 1). These results indicate that

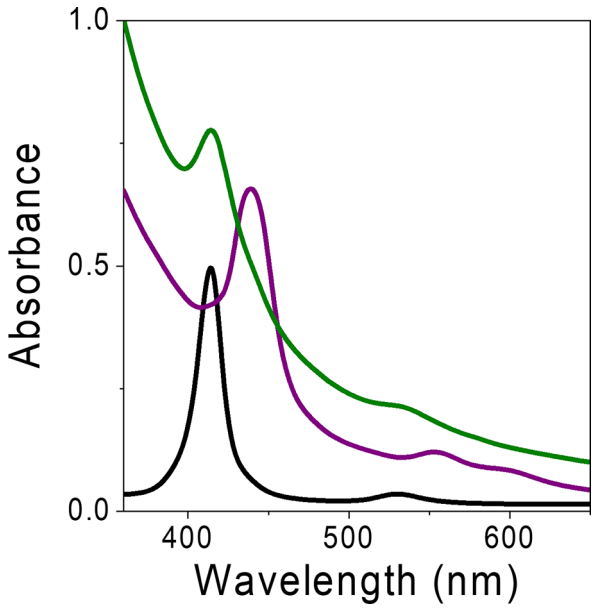

Figure 2. Absorption spectra of **CoP|nanoITO** (green), **CoTTP|PVP|nanoITO** (purple), and solution-dissolved **2** (black) in propylene carbonate.

the electronic transitions associated with cobalt porphyrins immobilized on nanoITO surfaces using the 4-vinylphenyl attachment chemistry are similar to those measured using homogeneous solutions of cobalt porphyrins, and, in both cases, the cobalt centers are predominately in a +2 oxidation state.

In contrast to the two absorption features observed in spectra of **CoP|nanoITO**, spectra of **CoTTP|PVP|nanoITO** samples collected in propylene carbonate display three distinct

Table 1. Absorption Maxima of Porphyrin Soret and Q-Type Transitions in Homogeneous Solutions of 1 and 2 as well as the Heterogeneous−Homogeneous Constructs: CoP|nanoITO and CoTTP|PVP|nanoITO[a]

construct/compound	absorption maxima	
	Soret band(s) (nm)	Q-band(s) (nm)
1 homogeneous	418	534
2 homogeneous	414	530
2 with excess pyridine (100 000 equiv) homogeneous	416 and 439	553 and 589
CoP|nanoITO heterogeneous−homogeneous	414	533
CoTTP|PVP|nanoITO heterogeneous−homogeneous	439	555 and 592

[a]All spectra were collected in propylene carbonate.

absorption bands that are assigned to Soret transitions at 439 nm and Q-band transitions at 555 and 592 nm (Figures 2, S13, S14 and Table 1). These transitions occur at longer wavelengths than those observed in spectra of **CoP|nanoITO** electrodes immersed in propylene carbonate and in spectra of **2** dissolved in propylene carbonate but are consistent with those observed in spectra of cobalt porphyrins dissolved in propylene carbonate solutions containing excess pyridine (Figure S14). Changes in the electronic spectra of cobalt porphyrins when in the presence of pyridine and oxygen have been previously reported[43−47] and ascribed to axial coordination of a pyridine unit and a superoxide ion, generating a 6-coordinate Co metal center in a +3 oxidation state. In combination with the characterization obtained via GATR−FTIR and XP spectroscopies, our measurements confirm that the immobilized cobalt porphyrins are coordinated to pyridyl groups of the surface-grafted polymers in the **CoTTP|PVP|nanoITO** constructs.

Electrochemical Analysis. Cyclic voltammograms recorded using customized working electrodes composed from either **CoP|nanoITO** or **CoTTP|PVP|nanoITO** were collected in propylene carbonate containing 0.1 M tetrabutylammonium perchlorate (TBAP) as the supporting electrolyte (see the Experimental Section for details). In this report, the cobalt porphyrin redox processes are for simplicity indicated as being metal centered; however, electron-transfer reactions involving metalloporphyrins have been ascribed to both innocent and noninnocent ligand chemistry.[48−51]

Cyclic voltammograms recorded using **CoP|nanoITO** electrodes display two 1-electron redox processes with midpoint potentials ($E_{1/2}$) of +0.15 and −1.19 V vs Fc^+/Fc that are assigned to $Co^{III/II}$ and $Co^{II/I}$ redox couples, respectively (Figure 3 and Table 2). Further, the anodic and cathodic peak currents of the $Co^{II/I}$ couple increase linearly with the scan rate, indicating the redox active species are surface-immobilized (Figure S15). For comparison, cyclic voltammograms recorded using a glassy carbon working electrode and homogeneous solutions of **2** (0.05 mM porphyrin in propylene carbonate with 0.1 M TBAP as the supporting electrolyte) display $Co^{III/II}$ and $Co^{II/I}$ redox features with midpoint potentials identical to those measured in experiments using **CoP|nanoITO** working electrodes (Figure S16 and Table 2).

Cyclic voltammograms collected using **CoTTP|PVP|nanoITO** electrodes also display redox features associated with $Co^{III/II}$ and $Co^{II/I}$ redox processes when measured under

DOI: 10.1021/acsami.9b15286
ACS Appl. Mater. Interfaces XXXX, XXX, XXX−XXX

experimental conditions identical to those used in experiments involving **CoP|nanoITO** electrodes, albeit with midpoint potentials measured at −0.20 and −1.34 V vs Fc^+/Fc, respectively (Figure 3 and Table 2). Likewise, the peak

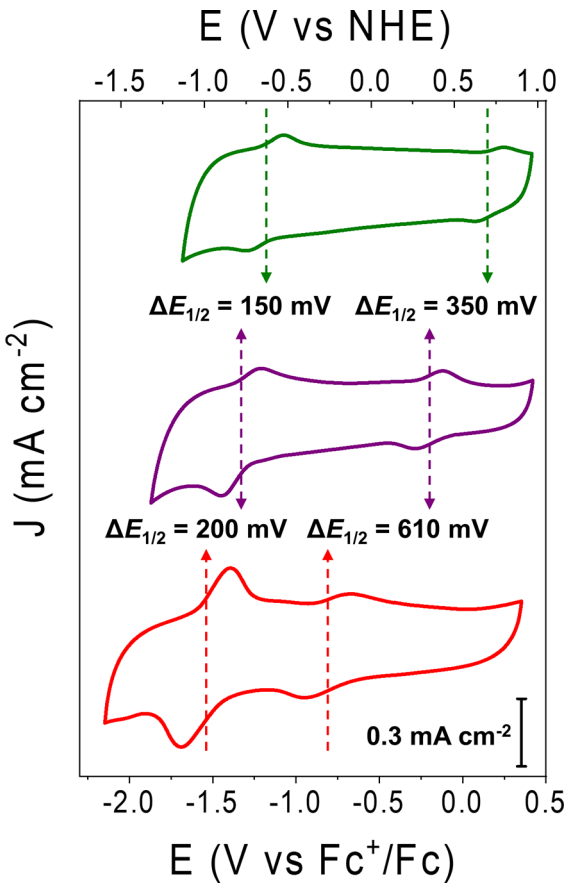

Figure 3. Cyclic voltammograms of **CoP|nanoITO** (green), **CoTTP|PVP|nanoITO** (purple), and **cobaloxime|PVP|nanoITO** (red) recorded in propylene carbonate containing 0.1 M TBAP as the supporting electrolyte under argon at a scan rate of 100 mV s^{-1}. The dashed vertical lines indicate the midpoint potentials of either the $Co^{III/II}$ or $Co^{II/I}$ redox couples associated with each construct.

currents associated with the $Co^{II/I}$ couple vary linearly with the scan rate, providing evidence that the redox features are also associated with surface-immobilized species (Figure S17). The offset of the cobalt porphyrin redox couples to more-negative values ($\Delta E_{1/2}$ of 350 and 150 mV for the $Co^{III/II}$ and $Co^{II/I}$ couples, respectively, as compared to those measured using **CoP|nanoITO** working electrodes or homogeneous solutions of **2**) is consistent with porphyrin immobilization via coordination to pyridyl groups of the surface-grafted polymers and electrochemical measurements performed in our laboratories (Figure S18) showing that the midpoint potentials measured using homogeneous solutions containing **2** appear at significantly more-negative values when excess pyridine is present (Figure S18 and Table S1). For example, at a cobalt porphyrin/pyridine ratio of 1:500, the midpoint potentials of the $Co^{III/II}$ and $Co^{II/I}$ redox couples are −0.60 and −1.29 V vs Fc^+/Fc, respectively, which are 750 and 100 mV more negative than the cobalt porphyrin midpoint potentials measured in the absence of pyridine (+0.15 and −1.19 V vs Fc^+/Fc, respectively).

Table 2. $Co^{III/II}$ and $Co^{II/I}$ Midpoint Potentials ($E_{1/2}$) of Homogeneous Solutions of 1, 2, and a Model Cobaloxime Complex ($Co(dmgH)_2PyCl$) as well as the Heterogeneous−Homogeneous Constructs: CoP|nanoITO, CoTTP|PVP|nanoITO, and cobaloxime|PVP|nanoITO[a]

construct/compound	$E_{1/2}$ of $Co^{III/II}$ V vs Fc^+/Fc	$E_{1/2}$ of $Co^{II/I}$ V vs Fc^+/Fc
1 homogeneous	+0.07	−1.16
2 homogeneous	+0.15	−1.19
2 with excess pyridine (500 equiv) homogeneous	−0.60	−1.29
$Co(dmgH)_2PyCl$ homogeneous	N/A[b]	−1.46
CoP|nanoITO heterogeneous−homogeneous	+0.15	−1.19
CoTTP|PVP|nanoITO heterogeneous−homogeneous	−0.20	−1.34
cobaloxime|PVP|nanoITO heterogeneous−homogeneous	−0.81	−1.54

[a]All voltammograms were recorded at a scan rate of 100 mV s^{-1} in propylene carbonate containing 0.1 M TBAP as the supporting electrolyte under argon at room temperature. [b]A chemically irreversible couple (i_a/i_c = 0.2) is observed with anodic and cathodic peaks at −0.60 and −0.90 V vs Fc^+/Fc, respectively.

In comparison with the porphyrin-based assemblies described in this work, previously reported **cobaloxime|PVP|nanoITO** electrodes studied under otherwise identical conditions require significantly more-negative bias potentials to access the $Co^{III/II}$ and $Co^{II/I}$ redox couples ($E_{1/2}$ of −0.81 and −1.54 V vs Fc^+/Fc, respectively) (Figure 3 and Table 2). These results demonstrate that cobalt centers immobilized onto an electrode can span nearly a volt in potential depending on their coordination environment and the chemical nature of how they are immobilized onto the surface.

Analysis of Cobalt Porphyrin Surface Loadings. Integration of the $Co^{II/I}$ redox waves in cyclic voltammograms recorded using either **CoP|nanoITO** or **CoTTP|PVP|nanoITO** electrodes suspended in propylene carbonate indicates that these samples contain 1.9 (±0.2) and 3.8 (±0.8) nmol of electroactive cobalt porphyrin species cm^{-2}, respectively. However, the total amount of cobalt present on surfaces of **CoP|nanoITO** and **CoTTP|PVP|nanoITO** as determined via ICP-MS is 4.1 (±0.2) and 15 (±3) nmol Co cm^{-2}, respectively.[52] In these examples, use of the polymeric architecture results in both a higher number of total and electroactive surface-immobilized cobalt porphyrins; however, there is a larger ratio of electroactive to total cobalt in the **CoP|nanoITO** samples (50% (±12%) vs 27% (±6%)). Thus, while the polymer grafting method affords increased porphyrin loadings, electrochemical measurements performed in propylene carbonate show that a smaller fraction of the porphyrins is electroactive. These results may be due to (1) a fraction of the metalloporphyrins is redox inactivated following immobilization on the heterogeneous nanoITO support and/or (2) a fraction of the metalloporphyrins is immobilized on areas of nanoITO that are electronically isolated from the working electrode. Also, in the case of using this heterogeneous−homogeneous design concept for electrocatalytic applications, the percentage of electroactive sites may not necessary equal the percentage of catalytically active sites, because reactions occurring at porous film coatings (including polymeric materials) require diffusion of the substrate and product through the film as well as management of charge-transfer processes.[53−55] We note the peak-to-peak separation for the

DOI: 10.1021/acsami.9b15286
ACS Appl. Mater. Interfaces XXXX, XXX, XXX−XXX

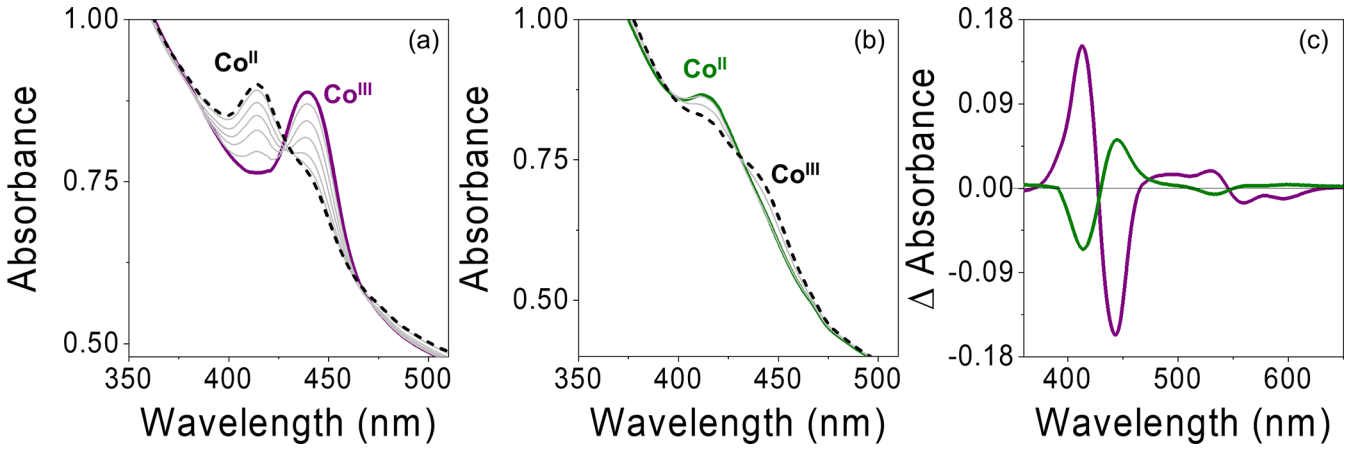

Figure 4. Absorption spectra of (a) **CoTTP|PVP|nanoITO** at open circuit potential (purple solid) and polarized at potentials required to generate the Co^{II} species (black dashed) as well as (b) **CoP|nanoITO** at open circuit potential (green solid) and polarized at potentials required to generate the Co^{III} species (black dashed). (c) Delta absorption spectra of **CoTTP|PVP|nanoITO** (purple solid) and **CoP|nanoITO** (green solid) after subtracting the colored spectra (initial) from the black dashed spectra (final) from panel (a) and panel (b). All spectra were collected in propylene carbonate containing 0.1 M TBAP as the supporting electrolyte under argon.

immobilized porphyrin redox features increases at faster scan rates, because internal resistance of the nanoITO film limits the rate of electron transfer.[39,56] Nonetheless, the ability to modulate the midpoint potential of a molecular catalyst using soft-material environments provides a strategy for better matching the redox thermodynamics of a targeted substrate/catalyst pair.

Spectroelectrochemistry. Polarization of **CoTTP|PVP|nanoITO** electrodes at potentials negative of the $Co^{III/II}$ redox couple generates Co^{II} species with spectral features similar to those observed in experiments using **CoP|nanoITO** electrodes under no polarization (Figure 4a,c). Similarly, polarization of **CoP|nanoITO** electrodes at potentials positive of the $Co^{II/I}$ redox couple generates Co^{III} species with spectral features similar to those observed in experiments using **CoTTP|PVP|nanoITO** electrodes under no polarization (Figure 4b,c).

Further analysis of these spectroelectrochemistry results reveals that a fraction of the spectral features recorded using **CoP|nanoITO** or **CoTTP|PVP|nanoITO** assemblies prior to any polarization contributes to the optical density following applied constant potential polarization. For experiments performed at sufficiently large bias potentials, the percentage of this contribution reaches a limiting value that is independent of applying any further bias. These "remnant" absorption features are assigned to cobalt porphyrin species on the surface that are electrochemically inactive and/or are immobilized on areas of nanoITO that are electronically isolated from the working electrode and do not convert between reduced and oxidized porphyrin species during polarization experiments. Comparisons of the Δ absorbance values at 414 nm between spectra recorded using **CoP|nanoITO** working electrodes prior to polarization (Figure 4b, green solid) and after applying sufficient positive polarization to oxidize all electroactive cobalt porphyrin species (Figure 4b, black dashed) (Figure S19) indicate 51% (±5%) of the cobalt porphyrin species on the surface are electroactive.[57] In contrast, comparison of the Δ absorbance values at 439 nm between spectra recorded using **CoTTP|PVP|nanoITO** working electrodes prior to polarization (Figure 4a, purple solid) and after applying sufficient negative polarization to reduce all electroactive cobalt porphyrin species (Figure 4a, black dashed) (Figure S19) indicate 31% (±7%) of the cobalt porphyrin species on the surface are electroactive.[57] These values are in good agreement with the ratio of total to electroactive cobalt loadings determined via ICP-MS measurements and integration of the $Co^{II/I}$ redox waves measured via cyclic voltammetry (vide supra).

CONCLUSIONS

Using either covalent attachment of a 4-vinylphenyl surface-grafting functional group or coordination to a polymeric interface, cobalt porphyrins have been immobilized onto a transparent and conductive oxide surface, enabling direct optical and electrochemical measurement of the porphyrin components used in these distinct constructs. The molecular interfaces provide a bioinspired strategy for preparing heterogeneous−homogeneous materials that enable modulation of the physical properties associated with the embedded metal centers. As compared to surface functionalization strategies based on drop-casting techniques, rationally designed molecular interfaces offer opportunities to organize and control the properties of surface coatings at the nanoscale. The constructs described in this report set the stage for analysis aimed at better understanding structure-function relationships governing hybrid heterogeneous−homogeneous materials.

EXPERIMENTAL SECTION

Materials. All reagents were purchased from Sigma-Aldrich. Dichloromethane, hexanes, methanol, and toluene were freshly distilled before use. Milli-Q water (18.2 MΩ cm) was used to prepare all aqueous solutions. ITO-coated glass slides and ITO nanopowder were purchased from Sigma-Aldrich. The ITO coatings are between 120 and 160 nm thick and have a resistivity of 8−12 Ω sq^{-1}. The nanopowder ITO has a particle size <50 nm and a surface area of 27 m^2 g^{-1}.

Synthesis. The compounds 5,10,15,20-tetra-*p*-tolyl-2-(4-vinylphenyl)porphyrin cobalt(II) (**1**) and 5,10,15,20-tetra-*p*-tolylporphyrin cobalt(II) (**2**) were synthesized using previously reported procedures. Further details are available as the Supporting Information.

Planar ITO Preparation. Unless otherwise noted, planar ITO-coated glass slides were cut into approximately 1 cm × 2 cm slides. All slides were initially degreased with an acetone-soaked cotton swab. ITO-coated glass slides were further cleaned using consecutive

DOI: 10.1021/acsami.9b15286
ACS Appl. Mater. Interfaces XXXX, XXX, XXX−XXX

ultrasonic treatments in two solvents (cleanroom isopropanol, 20 min, followed by acetone, 20 min). The slides were then dried under a stream of nitrogen and used immediately after cleaning.

NanoITO Preparation. Freshly cleaned ITO-coated glass slides were partially covered with Scotch tape, allowing the masked area to later serve as an uncoated surface for making electrical contacts. A previously reported coating procedure was used to coat the ITO slides with ITO nanoparticles via spin coating. Coated slides were placed on a hot plate (100 °C) for 2 min to drive off the excess solvent and then annealed under atmospheric pressure in a tube furnace at 350 °C.

Surface Functionalization via Polymer Grafting. ITO or nanoITO slides were placed into an argon-sparged solution of inhibitor-free 4-vinylpyridine and exposed to 254 nm UV light for 2 h. After thoroughly rinsing with methanol, the slides were dried under nitrogen and stored under vacuum. Cobalt porphyrin functionalization was achieved by covering the polymer-grafted slides with an argon-sparged solution of **2** (1 mM in each) in toluene and allowing to react for 18 h. The slides were then rinsed with toluene, followed by rinsing with cleanroom isopropanol, and drying under nitrogen and then vacuum.

Surface Functionalization via Structurally Modified Porphyrins. ITO or nanoITO slides were placed into a sealed quartz flask containing an argon-sparged solution of **1** in toluene (1 mM) and illuminated with shortwave UV light (254 nm) for 2 h. The porphyrin-functionalized slides are then removed from the flask, ultrasonically cleaned in toluene, rinsed with cleanroom isopropanol, and dried under nitrogen and then under vacuum.

Electrode Fabrication. ITO or nanoITO working electrodes were fabricated by connecting a copper clip with a copper wire using silver epoxy (Circuit Works). The copper clip/wire construct was passed through a glass tube, and the outside of the clip was insulated and attached to the glass tube with Loctite 615 Hysol Epoxi-patch adhesive. The epoxy was allowed to fully cure, and the clip was attached to the end of an electrode for testing.

Instrumentation. *UV−Vis.* Ultraviolet−visible (UV−vis) optical spectra were recorded on a Shimadzu SolidSpec-3700 spectrometer with a D_2 (deuterium) lamp for the ultraviolet range and a WI (halogen) lamp for the visible and near-infrared ranges.

FTIR. Grazing angle attenuated total reflection−Fourier transform infrared (GATR−FTIR) spectroscopy was performed using a VariGATR accessory (Harrick Scientific) with a Ge crystal plate installed in a Bruker Vertex 70 instrument. A minimum of three individual slides was tested for each sample. Samples were pressed against the Ge crystal to ensure effective optical coupling. Spectra were recorded under a dry nitrogen purge with a 4 cm^{-1} resolution, a GloBar MIR source, a broadband KBr beamsplitter, and a liquid nitrogen-cooled MCT detector. Background measurements were taken from the bare Ge crystal, and the data were processed using the OPUS software. Spectra from model compounds in pressed KBr pellets were recorded with the same settings but using transmission mode.

XPS. X-ray photoelectron spectroscopy (XPS) was performed using a monochromatized Al Kα source ($h\nu$ = 1486.6 eV), operated at 63 W, on a Kratos system at a takeoff angle of 0° relative to the surface normal and a pass energy for narrow scan spectra of 20 eV at an instrument resolution of approximately 700 meV. Survey spectra (40 scans) were recorded with a pass energy of 150 eV. A minimum of two individual slides was analyzed for each sample. Spectral fitting was performed using the Casa XPS analysis software, and all spectra were calibrated by adjusting the C 1s core-level position to 284.8 eV. Curves were fit with quasi-Voigt lines following Shirley background subtraction.

ICP-MS. Inductively coupled plasma mass spectroscopy (ICP-MS) measurements were conducted on a Thermo-Finnigan Neptune ICP-MS instrument. The samples were run in kinetic energy discrimination mode. The ICP-MS samples were prepared by immersing **CoP|nanoITO**, **CoTTP|PVP|nanoITO**, **PVP|nanoITO**, or unfunctionalized nanoITO electrodes in 1000 μL of a concentrated Omni trace H_2SO_4 solution and heating the solution at 60 °C for 20 min, followed by sonicating the solution for 1 h to ensure dissolution of the immobilized cobalt porphyrins into the solution. The mixture was then diluted to 6000 μL and sonicated for 1 h. The solution was then diluted with 0.1 M H_2SO_4 by taking 300 μL of the 6000 μL solution and diluting to 9180 μL. Three different samples were analyzed for **CoP|nanoITO**, **CoTTP|PVP|nanoITO**, **PVP|nanoITO** and unfunctionalized nanoITO substrates.

Electrochemistry. All cyclic voltammetry tests were performed with a Biologic potentiostat. All cyclic voltammograms recorded in organic solvents were obtained using a glassy carbon (3 mm diameter) disk or customized nanoITO working electrodes, a platinum counter electrode, and a silver wire pseudoreference electrode in a conventional three-electrode cell. Anhydrous propylene carbonate (Aldrich) was used as the solvent for electrochemical measurements. The supporting electrolyte was 0.1 M tetrabutylammonium perchlorate. The solution was sparged with argon. The working electrode was cleaned between experiments by polishing with an alumina (50 nm diameter) slurry, followed by solvent rinses. The potential of the pseudoreference electrode was determined using the ferrocenium/ferrocene redox couple as an internal standard and adjusted to the normal hydrogen electrode (NHE) scale (with $E_{1/2}$ taken to be 0.58 V vs the NHE in propylene carbonate).[58] In the case of quasi-reversible redox features, the midpoint potentials were estimated by taking the average of the anodic and cathodic peak potentials.

Spectroelectrochemistry. Measurements of **CoP|nanoITO** and **CoTTP|PVP|nanoITO** electrodes were recorded in anhydrous propylene carbonate using a **CoP|nanoITO** or **CoTTP|PVP|nanoITO** working electrode, a Pt wire counter electrode, and a silver wire pseudoreference electrode. The supporting electrolyte was 0.1 M tetrabutylammonium perchlorate. The solution was sparged with argon. The potential of the pseudoreference electrode was determined by measuring the ferrocenium/ferrocene redox couple under identical solvent conditions before and after completion of the measurements.

■ ASSOCIATED CONTENT

Supporting Information

The Supporting Information is available free of charge at https://pubs.acs.org/doi/10.1021/acsami.9b15286.

Synthesis and characterization of the cobalt porphyrin precursors; experimental methods; UV−vis and FTIR data as well as (spectro)electrochemical data (PDF)

■ AUTHOR INFORMATION

Corresponding Author

*E-mail: gfmoore@asu.edu.

ORCID

Brian L. Wadsworth: 0000-0002-0274-9993

Gary F. Moore: 0000-0003-3369-9308

Author Contributions

The manuscript was written through the contributions of all authors. All authors have given approval to the final version of the manuscript.

Funding

This research was supported by the National Science Foundation under the Early Career Award 1653982. B.L.W. was supported by an IGERT-SUN fellowship funded by the National Science Foundation (1144616) and the Phoenix Chapter of the ARCS Foundation.

Notes

The authors declare no competing financial interest.

■ ACKNOWLEDGMENTS

The authors gratefully acknowledge the use of facilities within the Eyring Materials Center at Arizona State University and

DOI: 10.1021/acsami.9b15286
ACS Appl. Mater. Interfaces XXXX, XXX, XXX−XXX

the W.M. Keck Foundation Laboratory for Environmental Biogeochemistry. We acknowledge Timothy Karcher from the Eyring Materials Center at Arizona State for assistance with XPS data collection and Gwyneth Gordon from the W.M. Keck Foundation Laboratory for Environmental Biogeochemistry for assistance with ICP-MS measurements.

■ ABBREVIATIONS

1, 5,10,15,20-tetra-*p*-tolyl-2-(4-vinylphenyl)porphyrin cobalt(II)
2, 5,10,15,20-tetra-*p*-tolylporphyrin cobalt(II)
ITO, indium tin oxide
nanoITO, nanostructured indium tin oxide
PVP, poly(vinylpyridine)
TCO, transparent conductive oxide
TBAP, tetrabutylammonium perchlorate
GATR–FTIR, grazing angle attenuated total reflectance Fourier transform infrared spectroscopy
XPS, X-ray photoelectron spectroscopy
UV–vis, ultraviolet–visible
ICP-MS, inductively coupled plasma mass spectrometry

■ REFERENCES

(1) Montoya, J. H.; Seitz, L. C.; Chakthranont, P.; Vojvodic, A.; Jaramillo, T. F.; Nørskov, J. K. Materials for Solar Fuels and Chemicals. *Nat. Mater.* **2017**, *16*, 70–81.
(2) Gust, D.; Moore, T. A.; Moore, A. L. Solar Fuels via Artificial Photosynthesis. *Acc. Chem. Res.* **2009**, *42*, 1890–1898.
(3) Xia, F.; Jiang, L. Bio-Inspired, Smart, Multiscale Interfacial Materials. *Adv. Mater.* **2008**, *20*, 2842–2858.
(4) Stamenkovic, V. R.; Strmcnik, D.; Lopes, P. P.; Markovic, N. M. Energy and Fuels from Electrochemical Interfaces. *Nat. Mater.* **2017**, *16*, 57–69.
(5) Mali, K. S.; Pearce, N.; De Feyter, S.; Champness, N. R. Frontiers of Supramolecular Chemistry at Solid Surfaces. *Chem. Soc. Rev.* **2017**, *46*, 2520–2542.
(6) Alexander, C.; Shakesheff, K. M. Responsive Polymers at the Biology/Materials Science Interface. *Adv. Mater.* **2006**, *18*, 3321–3328.
(7) Li, G.; Zhu, R.; Yang, Y. Polymer Solar Cells. *Nat. Photonics* **2012**, *6*, 153–161.
(8) Hou, J.; Inganäs, O.; Friend, R. H.; Gao, F. Organic Solar Cells Based on Non-Fullerene Acceptors. *Nat. Mater.* **2018**, *17*, 119–128.
(9) Günes, S.; Neugebauer, H.; Sariciftci, N. S. Conjugated Polymer-Based Organic Solar Cells. *Chem. Rev.* **2007**, *107*, 1324–1338.
(10) Liu, Y.; Li, C.; Ren, Z.; Yan, S.; Bryce, M. R. All-Organic Thermally Activated Delayed Fluorescence Materials for Organic Light-Emitting Diodes. *Nat. Rev. Mater.* **2018**, *3*, No. 18020.
(11) Farinola, G. M.; Ragni, R. Electroluminescent Materials for White Organic Light Emitting Diodes. *Chem. Soc. Rev.* **2011**, *40*, 3467–3482.
(12) Kalyani, N. T.; Dhoble, S. J. Organic Light Emitting Diodes: Energy Saving Lighting Technology—A Review. *Renewable Sustainable Energy Rev.* **2012**, *16*, 2696–2723.
(13) Kibsgaard, J.; Chen, Z.; Reinecke, B. N.; Jaramillo, T. F. Engineering the Surface Structure of MoS_2 to Preferentially Expose Active Edge Sites for Electrocatalysis. *Nat. Mater.* **2012**, *11*, 963–969.
(14) Lin, S.; Diercks, C. S.; Zhang, Y. B.; Kornienko, N.; Nichols, E. M.; Zhao, Y.; Paris, A. R.; Kim, D.; Yang, P.; Yaghi, O. M.; Chang, C. J. Covalent Organic Frameworks Comprising Cobalt Porphyrins for Catalytic CO_2 Reduction in Water. *Science* **2015**, *349*, 1208–1213.
(15) Hu, S.; Shaner, M. R.; Beardslee, J. A.; Lichterman, M.; Brunschwig, B. S.; Lewis, N. S. Amorphous TiO_2 Coatings Stabilize Si, GaAs, and GaP Photoanodes for Efficient Water Oxidation. *Science* **2014**, *344*, 1005–1009.
(16) Kanan, M. W.; Nocera, D. G. In Situ Formation of an Oxygen-Evolving Catalyst in Neutral Water Containing Phosphate and Co^{2+}. *Science* **2008**, *321*, 1072–1075.
(17) Shan, B.; Vanka, S.; Li, T. T.; Troian-Gautier, L.; Brennaman, M. K.; Mi, Z.; Meyer, T. J. Binary Molecular-Semiconductor p–n Junctions for Photoelectrocatalytic CO_2 Reduction. *Nat. Energy* **2019**, *4*, 290–299.
(18) Le Goff, A.; Artero, V.; Jousselme, B.; Tran, P. D.; Guillet, N.; Métayé, R.; Fihri, A.; Palacin, S.; Fontecave, M. From Hydrogenases to Noble Metal–Free Catalytic Nanomaterials for H_2 Production and Uptake. *Science* **2009**, *326*, 1384–1387.
(19) Gu, J.; Yan, Y.; Young, J. L.; Steirer, K. X.; Neale, N. R.; Turner, J. A. Water Reduction by a p-$GaInP_2$ Photoelectrode Stabilized by an Amorphous TiO_2 Coating and a Molecular Cobalt Catalyst. *Nat. Mater.* **2016**, *15*, 456–460.
(20) Wadsworth, B. L.; Khusnutdinova, D.; Moore, G. F. Polymeric Coatings for Applications in Electrocatalytic and Photoelectrosynthetic Fuel Production. *J. Mater. Chem. A* **2018**, *6*, 21654–21665.
(21) Jackson, M. N.; Oh, S.; Kaminsky, C. J.; Chu, S. B.; Zhang, G.; Miller, J. T.; Surendranath, Y. Strong Electronic Coupling of Molecular Sites to Graphitic Electrodes via Pyrazine Conjugation. *J. Am. Chem. Soc.* **2018**, *140*, 1004–1010.
(22) Queyriaux, N.; Kaeffer, N.; Morozan, A.; Chavarot-Kerlidou, M.; Artero, V. Molecular Cathode and Photocathode Materials for Hydrogen Evolution in Photoelectrochemical Devices. *J. Photochem. Photobiol., C* **2015**, *25*, 90–105.
(23) Buriak, J. M. Organometallic Chemistry on Silicon and Germanium Surfaces. *Chem. Rev.* **2002**, *102*, 1271–1308.
(24) McKone, J. R.; Marinescu, S. C.; Brunschwig, B. S.; Winkler, J. R.; Gray, H. B. Earth-Abundant Hydrogen Evolution Electrocatalysts. *Chem. Sci.* **2014**, *5*, 865–878.
(25) Lemberg, R.; Barrett, J. *Cytochromes*; Academic Press: London/New York, 1973.
(26) Cusanovich, M. A.; Meyer, T. E.; Tollin, G. Heme Proteins. *Adv. Inorg. Biochem.* **1988**, *7*, 37–91.
(27) Churg, A. K.; Weiss, R. M.; Warshel, A.; Takano, T. J. On the Action of Cytochrome c: Correlating Geometry Changes Upon Oxidation with Activation Energies of Electron Transfer. *J. Phys. Chem. A.* **1983**, *87*, 1683–1694.
(28) Gunner, M. R.; Honig, B. Electrostatic Control of Midpoint Potentials in the Cytochrome Subunit of the *Rhodopseudomonas viridis* Reaction Center. *Proc. Natl. Acad. Sci. U.S.A.* **1991**, *88*, 9151–9155.
(29) Mao, J.; Hauser, K.; Gunner, M. R. How Cytochromes with Different Folds Control Heme Redox Potentials. *Biochemistry* **2003**, *42*, 9829–9840.
(30) Mauk, A. G.; Moore, G. R. Control of Metalloprotein Redox Potentials: What Does Site-Directed Mutagenesis of Hemoproteins Tell Us? *J. Biol. Inorg. Chem.* **1997**, *2*, 119–125.
(31) Armstrong, F. A.; Hirst, J. Reversibility and Efficiency in Electrocatalytic Energy Conversion and Lessons from Enzymes. *Proc. Natl. Acad. Sci. U.S.A.* **2011**, *108*, 14049–14054.
(32) Hambourger, M.; Moore, G. F.; Kramer, D. M.; Gust, D.; Moore, A. L.; Moore, T. A. Biology and Technology for Photochemical Fuel Production. *Chem. Soc. Rev.* **2009**, *38*, 25–35.
(33) Cracknell, J. A.; Vincent, K. A.; Armstrong, F. A. Enzymes as Working or Inspirational Electrocatalysts for Fuel Cells and Electrolysis. *Chem. Rev.* **2008**, *108*, 2439–2461.
(34) Tran, P. D.; Artero, V.; Fontecave, M. Water Electrolysis and Photoelectrolysis on Electrodes Engineered Using Biological and Bio-Inspired Molecular Systems. *Energy Environ. Sci.* **2010**, *3*, 727–747.
(35) Smith, S. E.; Yang, J. Y.; DuBois, D. L.; Bullock, R. M. Reversible Electrocatalytic Production and Oxidation of Hydrogen at Low Overpotentials by a Functional Hydrogenase Mimic. *Angew. Chem., Int. Ed.* **2012**, *51*, 3152–3155.
(36) Khusnutdinova, D.; Beiler, A. M.; Wadsworth, B. L.; Jacob, S. I.; Moore, G. F. Metalloporphyrin-Modified Semiconductors for Solar Fuel Production. *Chem. Sci.* **2017**, *8*, 253–259.
(37) Beiler, A. M.; Khusnutdinova, D.; Wadsworth, B. L.; Moore, G. F. Cobalt Porphyrin–Polypyridyl Surface Coatings for Photo-

DOI: 10.1021/acsami.9b15286
ACS Appl. Mater. Interfaces XXXX, XXX, XXX–XXX

electrosynthetic Hydrogen Production. *Inorg. Chem.* **2017**, *56*, 12178−12185.
(38) Wadsworth, B. L.; Beiler, A. M.; Khusnutdinova, D.; Reyes Cruz, E. A.; Moore, G. F. Interplay between Light Flux, Quantum Efficiency, and Turnover Frequency in Molecular-Modified Photoelectrosynthetic Assemblies. *J. Am. Chem. Soc.* **2019**, *141*, 15932−15941.
(39) Wadsworth, B. L.; Beiler, A. M.; Khusnutdinova, D.; Jacob, S. I.; Moore, G. F. Electrocatalytic and Optical Properties of Cobaloxime Catalysts Immobilized at a Surface-Grafted Polymer Interface. *ACS Catal.* **2016**, *6*, 8048−8057.
(40) Khusnutdinova, D.; Beiler, A. M.; Wadsworth, B. L.; Nanyangwe, S. K.; Moore, G. F. Vibrational Structure Analysis of Cobalt Fluoro-Porphyrin Surface Coatings on Gallium Phosphide. *J. Porphyrins Phthalocyanines* **2018**, *22*, 461−466.
(41) Boucher, L. J.; Katz, J. J. The Infared Spectra of Metalloporphyrins (4000−160 cm^{-1}). *J. Am. Chem. Soc.* **1967**, *89*, 1340−1345.
(42) Kincaid, J.; Nakamoto, K. Vibrational Spectra of Transition Metal Complexes of Tetraphenylporphine. *J. Inorg. Nucl. Chem.* **1975**, *37*, 85−89.
(43) Walker, F. A. Electron Spin Resonance Study of Coordination to the Fifth and Sixth Positions of $\alpha,\beta,\gamma,\delta$-Tetra(p-methoxyphenyl)-porphinatocobalt (II). *J. Am. Chem. Soc.* **1970**, *92*, 4235−4244.
(44) Walker, F. A. Steric and Electronic Effects in the Coordination of Amines to a Cobalt (II) Porphyrin. *J. Am. Chem. Soc.* **1973**, *95*, 1150−1153.
(45) Walker, F. A. Reactions of Monomeric Cobalt-Oxygen Complexes. I. Thermodynamics of Reaction of Molecular Oxygen with Five-and Six-Coordinate Amine Complexes of a Cobalt Porphyrin. *J. Am. Chem. Soc.* **1973**, *95*, 1154−1159.
(46) Jones, R. D.; Summerville, D. A.; Basolo, F. Synthetic Oxygen Carriers Related to Biological Systems. *Chem. Rev.* **1979**, *79*, 139−179.
(47) Yang, J.; Huang, P. A Study of Cobalt (II) Porphyrins on Their Oxygen-Binding Behaviors and Oxygen-Facilitated Transport Properties in Polymeric Membranes. *Chem. Mater.* **2000**, *12*, 2693−2697.
(48) Kadish, K. M.; Van Caemelbecke, E. Electrochemistry of Porphyrins and Related Macrocycles. *J. Solid State Electrochem.* **2003**, *7*, 254−258.
(49) Sun, H.; Smirnov, V. V.; DiMagno, S. G. Slow Electron Transfer Rates for Fluorinated Cobalt Porphyrins: Electronic and Conformational Factors Modulating Metalloporphyrin ET. *Inorg. Chem.* **2003**, *42*, 6032−6040.
(50) Lyaskovskyy, V.; de Bruin, B. Redox Non-Innocent Ligands: Versatile New Tools to Control Catalytic Reactions. *ACS Catal.* **2012**, *2*, 270−279.
(51) Luca, O. R.; Crabtree, R. H. Redox-Active Ligands in Catalysis. *Chem. Soc. Rev.* **2013**, *42*, 1440−1459.
(52) Unlike 4-vinylpyridine, the UV-induced grafting of **1** on planar gallium phosphide substrates yields surface coverages inconsistent with formation of dense polymer brushes (see ref 36), and instead indicate near monolayer surfaces coverages (0.59 ± 0.03 nmol cm^{-2}). In the current work, the loadings and relatively high surface area of the nanoITO complicate an analogous assessment. However, if some polymerized forms of **1** are present on the nanoITO supports, this would not change the measured per-metal-site loadings or invalidate interpretations that an initially applied polymeric surface graft can provide coordination sites to assemble metallocomplexes and control their electrochemical properties.
(53) Andrieux, C. P.; Dumas-Bouchiat, J. M.; Savéant, J. M. Kinetics of Electrochemical Reactions Mediated by Redox Polymer Films: New Formulation and Strategies for Analysis and Optimization. *J. Electroanal. Chem. Interfacial Electrochem.* **1984**, *169*, 9−21.
(54) Costentin, C.; Savéant, J. M. Cyclic Voltammetry Analysis of Electrocatalytic Films. *J. Phys. Chem. C* **2015**, *119*, 12174−12182.
(55) Costentin, C.; Savéant, J. M. Molecular Approach to Catalysis of Electrochemical Reaction in Porous Films. *Curr. Opin. Electrochem.* **2019**, *15*, 58−65.
(56) Chen, Z.; Concepcion, J. J.; Hull, J. F.; Hoertz, P. G.; Meyer, T. J. Catalytic Water Oxidation on Derivatized nanoITO. *Dalton Trans.* **2010**, *39*, 6950−6952.
(57) Spectral contributions from the underpinning ITO were subtracted from the spectra collected both prior to and following polarization.
(58) Connelly, N. G.; Geiger, W. E. Chemical Redox Agents for Organometallic Chemistry. *Chem. Rev.* **1996**, *96*, 877−910.

DOI: 10.1021/acsami.9b15286
ACS Appl. Mater. Interfaces XXXX, XXX, XXX−XXX